Appendix B

DETECTION OF SNOW AND VEGETATION COVER USING MILLIMETER-WAVE IMAGING RADIOMETER (MIR) DATA

Andrew Tait[1]

Dorothy Hall[2]

Jim Foster[2]

Al Chang[2]

Andrew Klein[1]

1 Universities Space Research Association, Code 974, NASA/Goddard Space Flight Center, Greenbelt, MD 20771, Ph (301) 286-6020, FAX (301) 286-1758, e-mail : atait@glacier.gsfc.nasa.gov

2 Hydrological Sciences Branch, Code 974, NASA/Goddard Space Flight Center, Greenbelt, MD 20771

Submitted to Remote Sensing of Environment

ABSTRACT

Millimeter-wave Imaging Radiometer (MIR) data (ranging in frequency from 89 to 325 GHz) collected from NASA ER-2 flights over the Great Lakes region, New England, and Ontario in February 1997, are used to identify vegetation and snow cover. A Normalized Difference Vegetation Index (NDVI), derived from Advanced Very High Resolution Radiometer (AVHRR) data, is used to determine vegetation type. Snow and cloud cover are obtained using the Moderate Resolution Imaging Spectroradiometer (MODIS) snow mapping and cloud masking algorithms performed on MODIS Airborne Simulator (MAS) data. Results show that for cloud-free scenes, the MIR atmospheric window channels (89, 150, and 220 GHz) are well related to the snow and vegetation cover, which are also strongly related to each other. Furthermore, there is some indication that the variability within the MIR data may be related to patchy snow and percent forest-covered area. Under cloudy conditions the MODIS snow mapping algorithm is unable to detect snow on the surface. However, it is shown that surface features are clearly discernible using millimeter-wave radiation data at 89 GHz. The number of snow-covered MIR pixels for the flight on 9 February 1997 increased by 33.33% when using the 89 GHz data compared with the MODIS snow algorithm. This corresponds very closely with the percent cloud cover for this flightline, which is 34.40%. A snow cover model is developed using these 89 GHz data and surface air temperature data obtained from the NOAA Climate Diagnostics Center (CDC) reanalysis. The model is tested on a different flightline and is shown to be effective for the detection of snow-cover under clear and cloudy conditions over this area. It is

suggested, though, that this model may not be suitable for all regions and for all times of the year.

INTRODUCTION

Snow and vegetation cover are important factors in Earth systems science. Due to its high albedo, high thermal emissivity, and low thermal conductivity, snow cover strongly influences the overlying atmosphere (Chang *et al.*, 1985). Evidence suggests that anomalies of the snow cover might induce complex feedback mechanisms leading to local and global climate fluctuations (Hahn and Shukla, 1976; Walsh and Ross, 1988). Snow cover is also a key component in the global hydrological cycle, however knowledge of global snow-covered area from surface-based measurements is limited due to large gaps in recording networks. Vegetation cover impacts both the atmosphere and land surface through its albedo, interception and transpiration of water, emissions of trace greenhouse gases such as methane and carbon-dioxide, oxygen cycling, and nutrient exchanges with the soil (Townshend *et al.*, 1993). Furthermore, changes in land cover have considerable implications for ecosystems, biogeochemical fluxes, and climate (IGBP, 1990).

Satellite-derived snow and vegetation cover maps are important for monitoring changes in these phenomena at the synoptic- (around 1000 km^2) to the global-scale. In addition, knowledge of the snow and vegetation cover is vital for improving large-scale hydrological models, refining medium- and long-range weather forecasts, and for perfecting general circulation models (Rango, 1985). Long-term changes in snow and vegetation cover may also indicate responses to climate change.

Snow-covered area is often derived from satellite-attained reflected visible radiation data in the wavelength range (0.38 to 0.71 microns). This is due to the high albedo of snow (0.40 to 0.95) compared with soil (0.05 to 0.40) and vegetation (0.05 to 0.26). Near infrared radiation data (0.71 to 4.0 microns) is also used as an indicator of snow-cover as variability in surface temperature is detectable at these wavelengths (Massom, 1991). Vegetation cover is mapped from the difference between visible and near infrared data. Red spectral measurements are inversely related to the chlorophyll content of vegetation while near infrared measurements are directly related to the mesophyll structure of leaves (Townshend *et al.*, 1993). Both of these methods, though, are largely dependent upon daytime cloud-free scenes, which limit data retrieval. Passive microwave radiation (0.1 to 30 centimeters) is largely transparent to atmospheric water vapor and clouds, particularly at wavelengths greater than around 0.8 cm, and can be detected in all lighting conditions. However, due to constrictions on the antenna size of satellite passive microwave instruments, such as the Special Sensor Microwave Imager (SSM/I), the ground resolution at nadir is comparatively poor (45 by 70 km for the SSM/I 1.55 cm (19.4 GHz) channel compared with 0.5 to 1.0 km resolution for the data from visible and near infrared channels on the Advanced Very High Resolution Radiometer (AVHRR), for example).

This study analyzes the responses of millimeter-wave radiation under different snow and vegetation conditions as measured during the WINter Cloud Experiment (WINCE) in January and February 1997. These data may be used for detecting and monitoring snow and vegetation cover at a spatial resolution of around 14 by 16 km

(ground resolution at nadir for the SSM/I 3.5 mm (85 GHz) channel). The objective of this study is to examine the utility of passive millimeter-wave data, recorded by the Millimeter-wave Imaging Radiometer (MIR) instrument flown on the NASA ER-2 aircraft over Wisconsin, New York and New England in February 1997, for the purpose of distinguishing differences in snow and vegetation cover under clear and cloudy sky conditions. MIR data are used in combination with Moderate Resolution Imaging Spectroradiometer (MODIS) Airborne Simulator (MAS) data, International Geosphere-Biosphere Programme (IGBP) land-cover maps, NOAA Climate Diagnostics Center (CDC) reanalysis surface air temperature data, and ground-based snowpack information to evaluate the relationships between millimeter-wave brightness temperatures, snow and vegetation cover.

The MIR records radiation emanating from the surface and atmosphere in nine bands (Table 1). The bands were chosen to match those of the Advanced Microwave Sounding Unit-B (AMSU-B) planned for NOAA operational satellites and the Earth Observing System (EOS) PM1 platform, beginning in 2000. The MIR instrument was developed for atmospheric research, with the three channels centered about 183 and 325 GHz designed to study the atmospheric water vapor profile (Racette *et al.*, 1996). Other channels are less opaque and can provide some information about the surface. At an aircraft altitude of around 20,000 m the temperature sensitivity of the instrument is less than 1 K for all channels except those centered around 325 GHz, which were found to be ineffective for determining atmospheric or surface parameters (Wang, personal communication). The MIR pixel size is around 500 by 500 m at nadir. The

instrument has been flown on several NASA ER-2 missions, including the WINter Cloud Experiment (WINCE) in January and February 1997.

Between 23 January and 13 February 1997 the ER-2 flew on eleven separate occasions over Wisconsin, Michigan, New England, the Great Lakes and Ontario. The flight dates were January 23, 28, 29, 30, and February 2, 6, 8, 9, 10, 12 and 13. Along with the MIR, the aircraft carried several other instruments including the MAS, the Aerosol Particulate Sampler (APS), the High Resolution Interferometer Sounder (HIS), and the Cloud Lidar System (CLS). The overall mission objective was to use remotely-sensed data to learn more about detecting clouds from space in winter conditions. A specific objective on the 9 February 1997 flight was to overfly instrumentation sites near Oneonta, New York and Keene, New Hampshire for validation of MODIS snow-mapping algorithms under clear-sky conditions.

The surface cover in Wisconsin, Michigan and New England is typically cropland or natural vegetation interspersed with areas of deciduous broadleaf forest, according to the IGBP Land-Cover classification. This classification uses the Normalized Difference Vegetation Index (NDVI) derived from AVHRR 1 km data (Belward and Loveland, 1995). Over the period of the WINCE campaign, the snow conditions over the region remained fairly continuous, with an average snow depth of around 10 to 15 cm.

Hall *et al.* (1995) suggest that variations in surface vegetation may be detectable

under clear-sky conditions, due to differences in recorded millimeter-wave brightness temperatures between different species of vegetation. In addition, the MIR data may be used to estimate snow cover characteristics such as melting snow and snow-covered area. The onset of melt transforms a snowpack from one which scatters microwave radiation to one which absorbs and re-emits it (Ulaby and Stiles, 1980). This dramatically increases the brightness temperature (T_B) to that approaching the physical temperature of the medium. Also, Rango *et al.* (1979) show that when the snowpack is dry there is sufficient contrast in the brightness temperature range between snow and bare ground, due to a lower dielectric constant and the effect of scattering in snow, for estimation of snow-covered area.

Millimeter-wave radiation data are also sensitive to atmospheric water vapor and clouds (Gasiewski, 1992). Indeed, it is possible to detect clouds over water and snow-free land using data from the MIR instrument (Racette *et al.,* 1996). However, when the surface is covered with snow it is more difficult to distinguish the relatively low brightness temperatures associated with the clouds with the similarly low brightness temperatures associated with a snow cover (Chang *et al.*, 1987). The MIR instrument measures mixed polarization signals, rather than horizontal and vertical, therefore polarization ratios or differences cannot be used to discriminate clouds. If horizontal and vertical polarizations were measured, it may be possible to more readily identify clouds, as surface emissions tend to be polarized while in general there is no polarization information from clouds. Despite the sensitivity of millimeter-wave data to clouds, some surface information may still be obtained in cloudy conditions using the

less opaque MIR channels at 89, 150, and 220 GHz.

This study analyzes the MIR data recorded on 9 February 1997. A specific mission objective for this day was to overfly instrumentation sites in New York and New Hampshire where air and snowpack temperature, snow depth, snow density, and snow crystal characteristics were measured. These data are compared with the MIR and MAS measurements. Many of the New England scenes were cloud-free or had a few thin cirrus clouds present, while the Michigan section of the flightline had a continuous coverage of cumulus clouds. Hence, the relationships between millimeter-wave radiation, snow and vegetation cover are studied for varying cloud conditions.

DESCRIPTION OF ER-2 FLIGHT ON 9 FEBRUARY 1997

Figure 1 shows the ER-2 flightline for 9 February 1997 overlaid on a Geostationary Operational Environmental Satellite (GOES-8) visible image. The ER-2 aircraft left Madison, Wisconsin at 16:00 UTC (11:00 EST) and flew directly to the New York field site near Oneonta arriving around 17:30 UTC. Cloud conditions over Michigan were between 80 and 100 percent cumulus and cirrus. The aircraft proceeded to the New Hampshire field sites reporting clear skies across New England.

Time series of the mean across-track brightness temperature (T_B) for the three MIR atmospheric window channels (89, 150, and 220 GHz) are shown as Figure 2.

Some surface features are discernible, particularly the depression in the mean T_B over the Great Lakes caused by the low emissivity of water. The mean T_B is lower for lower frequencies due to the relationship between frequency and atmospheric absorption. Atmospheric absorptivity increases with increasing microwave frequency. This is because the number of energy states of water and oxygen molecules at which absorption of microwaves occurs increases as wavelength decreases (Reeves *et al.*, 1975). Using a simple radiative transfer model with a winter mid-latitude atmosphere, the atmospheric absorptivity at 89, 150, and 220 GHz is approximately 0.606, 0.704, and 0.760 respectively. From the conservation of energy, emissivity is equal to absorptivity. Hence, at higher microwave frequencies the brightness temperature is higher due to a larger contribution from atmospheric emission, principally from water vapor and oxygen.

ANALYSIS OF A CLOUD-FREE SCENE

Hall *et al.* (1995), using MIR data collected over Alaska in 1995, conclude that the MIR brightness temperature patterns are related to land cover. They state further that the major delineation appears along the boundary between black spruce forest and the meadow dryas. Coniferous trees emit more microwave radiation than do tundra or dryas vegetation, and this is one explanation for the higher brightness temperatures in the black spruce forests. Tait *et al.* (submitted) conclude that the optimum binary

classification of land cover using MIR data depends upon the condition of the snowpack (dry, melting, or patchy). This suggests that the combination of snow and vegetation cover generates a strong signal in the MIR data. These findings were replicated in this study.

Figure 3 is a side-by-side comparison of MIR, MAS, and IGBP vegetation data for a cloud-free section of the 9 February 1997 data near Ithaca, New York. The first three columns represent data from the 89, 150, and 220 GHz channels of the MIR instrument. The top scale shows the range of brightness temperatures from 180 to 270 K. The fourth column is the Channel 2 (0.627 microns) reflectance data from the MAS. The lower scale shows the reflectance range from 0.14 to 0.86. Note that the width of this and the next two columns is a little less than the MIR data, due to the different scan angles of the instruments (MIR = 100°, MAS = 85.92°). The data gap two-thirds through this scene is due to the aircraft making a turn.

The fifth column depicts the location of snow (in white) as mapped by the MODIS snow mapping algorithm (Klein *et al.*, 1998) used on the MAS data. Because the algorithm is based on optical data, no snow will be mapped under thick cloud cover. The sixth column shows the cloud cover as prescribed by the MAS cloud-masking algorithm (Ackerman *et al.*, 1997). Briefly, the cloud-masking algorithm initializes each scene as cloudy and then several threshold tests are performed to determine which pixels are clear. Based on known relationships, cloud type can also be distinguished as

either low or high cloud. There are also flags for day or night, sun glint, a snow or ice background, a land or water background, shadow, and an obstructed field of view (by smoke or dust, for example). Column six is almost 100% cloud-free (red). In blue are pixels which have been designated high cloud only, while the yellow pixels represent both high and low clouds and green pixels denote low cloud only.

Lastly, the IGBP NDVI-obtained vegetation is mapped. The pixels colored red through green are forested (red = evergreen needleleaf; yellow = deciduous broadleaf; green = mixed forest). The purple- and pink-colored areas are cropland and cropland/natural vegetation mosaic. White pixels are open water. Most of the land cover in this scene is deciduous broadleaf forest. From bottom to top the four lakes visible are Lakes Canadaigua, Keuka, Seneca, and Cayuga, at which the city of Ithaca is located on the south coast.

There is a distinct relationship between the MIR brightness temperatures, MAS channel 2 reflectance, snow cover, and the vegetation type. Much of the cropland is snow-free or has a patchy snow cover, while the forested regions are almost completely snow-covered. The MAS data show this relationship well, with reflectances as high as 0.86 in snow-covered areas and as low as 0.14 in snow-free areas. Likewise, the MIR data show brightness temperatures as low as 180 K (89 GHz) over the snow-covered areas and as high as 265 K (220 GHz) over the snow-free areas. The low brightness temperatures over the snow are associated with a lower physical temperature of the emitting medium and some scattering of the radiation from within the upper few

centimeters of the snowpack. Upon inspection of aerial photos over this scene, the cropland/natural vegetation areas appear to have a patchy or thin snow cover over a dark soil, while the forested areas have a continuous snow cover. This supports the reflectance and brightness temperature data. The uneven distribution of snow is due to a combination of the area's exposure and the amount of redistribution of snow by wind, and the low albedo of the dark soil which enhances the absorption of solar radiation leading to rapid melting of the snow.

It is shown that for a cloud-free scene, the MIR data at 89, 150, and 220 GHz are well related to the land and snow cover, which are also closely related to each other. From Figure 3, MIR brightness temperature variability within the forested and cropland areas can also be seen. It is hypothesized that some snow depth information may be discernible from this variability. Hence, the relationship between MIR brightness temperature data and snow depth was investigated using ground-based snowpack information from the field measurements.

COMPARISON WITH GROUND-BASED MEASUREMENTS

The field site near Oneonta NY is located in an area of mainly hemlock and birch trees with some open areas. Seventeen locations within the field site were visited on 9 February 1997 and measurements of percent snow cover, air and snow temperature, and snow depth were obtained. Also, the average snow grain size and the percent forest cover were estimated at each measurement site. Table 2 lists the location of the

measurements, the mean snow depth (cm), the estimated percent forest cover (%), and the corresponding MIR brightness temperature at 89 GHz (K). The field data from Keene, New Hampshire were not used in this study because latitude and longitude coordinates were not recorded. Thus, it was not possible to co-locate the ground and air data.

Figure 4 is a plot of brightness temperature at 89 GHz versus snow depth measured at the Oneonta field site. There is no relationship present. This may be because the penetration depth of microwave radiation at 89 GHz is between approximately 3 and 30 cm (10 to 100 times the wavelength), while the average snow depth at this site is around 11 cm. Hence the microwave signal may be originating from the upper layer of the snowpack only. This would result in a poor relationship between the total snow depth and brightness temperature. The observed variability in the MIR data is more closely related to the percent forest cover, as shown in Figure 5. It should be noted that the percent forest cover is only an estimate, derived from a ground-based visual impression of the tree density in the vicinity of the measurement. There is a positive relationship between brightness temperature and percent forest cover. As the tree density increases the emission from the trees increases and the radiation from the snowpack is partially absorbed and reemitted by the canopy. This results in higher brightness temperatures compared with low tree density areas. While further analysis of this relationship is required, incorporating more field measurements, this result shows the potential for mapping percent forest cover using microwave data.

It is hypothesized that the variability in the MIR data over cropland / natural

vegetation areas is caused by patchy snow. This is supported by aerial photos which show dark patches of exposed soil interspersed with highly reflective snow covered areas. In open areas such as these, patchy snow is not unusual due to the redistribution of snow by wind. If the surface has been tilled, snow will deposit in the furrows while the hummocks will be snow-free. Also, snow is deposited around clumps of natural grasses but may be absent from areas of very short vegetation or bare ground.

ANALYSIS OF A CLOUDY SCENE

The section of the ER-2 flight on 9 February 1997 over Michigan (from around 16:20 UTC to 16:45 UTC) was almost entirely cloud covered. It is during conditions such as this that microwave data should be most useful, to supplement the visible data. Surface features are clearly visible in the MIR data for this scene. Can the vegetation type or the presence of snow cover be detected?

Figure 6 is a side-by-side comparison of the MIR, MAS, and IGBP Land Cover data for the Michigan section of the flight. The color scheme is the same as that for Figure 3. The majority of the scene is covered by a combination of high and low cloud. The strip of cloud seen in the lower right of the cloud mask data is probably an aircraft contrail. Note that due to the extensive cloud cover, no snow is mapped by the MODIS snow-mapping algorithm. The surface cover is mainly cropland and natural vegetation,

with some areas of mixed forest.

Upon comparison with Figure 3, it can be seen that the visible reflectance of the clouds is very similar to that of snow (between around 0.60 to 0.80). This makes the automated discrimination between low clouds and snow cover very difficult. In addition, snow and low clouds have similar thermal properties in the near infrared portion of the electromagnetic spectrum (Allen *et al.*, 1990). Continuous cloud cover, as shown in Figure 6, also hampers the detection of snow and land cover using visible and near infrared radiation data because surface features cannot be detected. This study shows that millimeter-wave radiation can penetrate the cloud cover and be used to delineate surface features.

In Figure 6, the MIR data clearly show the shores of Lake Michigan, as well as the boundary between mixed forest and cropland/natural vegetation. It appears that the cloud cover has little impact upon the brightness temperature at 89 GHz. Atmospheric absorption and re-emission is more prevalent at the higher frequencies, hence those brightness temperatures are higher. The mean T_B at 89 GHz for the mixed forest pixels is 230 K. This compares well with the mean T_B for the snow-covered deciduous broadleaf forest pixels from the cloud-free Oneonta scene (T_B = 228 K), which suggests that the Michigan forest pixels are also snow covered. Furthermore, the mean T_B at 89 GHz for the cropland and natural vegetation pixels in the Michigan scene is 219 K, while the mean T_B at 89 GHz for the same land cover at Oneonta is 253 K. It is known that the Oneonta pixels are snow-free, therefore it is concluded that the cropland and

natural vegetation pixels in the Michigan scene are probably snow-covered.

A scheme for using MIR 89 GHz brightness temperature data to determine snow cover was developed using the data from the 9 February 1997 flight. This included data from cloudy as well as cloud-free scenes. The analysis was performed for forested and cropland/natural vegetation areas separately. Surface air temperature data, obtained from NOAA Climate Diagnostics Center (CDC) at a resolution of 2.5 by 2.5 degrees, were used to reduce the impact of spatial and temporal air temperature variability on the brightness temperature data. MIR brightness temperature data at 89 GHz were divided by the surface air temperature (T_B / T_{AIR}) for each pixel. These values formed the basis for determining snow-covered area. Cutoff values representing the least difference between the MIR-based snow map and the MODIS snow map for the 9 February 1997 flight were obtained. For this comparison, only cloud-free pixels were used. A cutoff of T_B / T_{AIR} = 0.8725 was used to delineate snow within cropland/natural vegetation areas. Pixels with values less than or equal to the cutoff were mapped as snow while pixels with higher values are snow-free. The same procedure was used for forested areas, resulting in a cutoff of T_B / T_{AIR} = 0.9712.

Figure 7 shows the difference between the two snow mapping methods for all the 9 February MIR scan lines. Zero values represent open water or periods when the aircraft was making a turn. All the large positive differences (greater than around 20 pixels per scan line) are due to the presence of cloud cover. During these cloudy periods, the MODIS snow mapping algorithm is unable to map snow while the MIR

instrument is still able to detect snow. The negative values are primarily in forested areas where the MIR algorithm is slightly under-estimating the snow cover. This is may be due to a masking of the snow signal by areas with a high percent forest cover (80 to 100 %). The total number of snow-covered pixels based on the MIR method is 538,468 compared with 403,860 pixels using the MODIS snow map, which represents an increase of 33.33% in the estimated snow-covered area. This corresponds very closely with the percent cloud cover for this flightline, 34.40%, which suggests that for cloud-free scenes the methods are very similar.

The MIR snow mapping algorithm was tested on data from the flight on 6 February 1997. This was a round-trip flight from Madison, Wisconsin crossing Lake Superior and traversing north to Hudson Bay and returning via a path over Lake Michigan. The vegetation cover is more varied on this flightline, ranging from large regions of evergreen needleleaf forests to areas of permanent wetland. The broadleaf forest cutoff ($T_B / T_{AIR} = 0.9712$) was used for all forest types and the cropland/natural vegetation cutoff ($T_B / T_{AIR} = 0.8725$) was used for all non-forested areas. Almost 100 % cumulus and cirrus cloud cover was present over the Great Lakes region and clear skies with scattered cirrus over most of Ontario. Figure 8 represents the MIR and MAS snow cover comparison for 6 February 1997.

It can be seen that for the cloudy periods of the flight, around scan number 1000 and 4500, the MIR-based method is able to map snow while the MAS-based algorithm is not. Over the cloud-free section, from around scan number 1500 to 4000, the two

methods are comparable. The negative values appear to be related to forested regions, where the MIR-method may be underestimating snow cover. The increase in snow-covered pixels is 43.51%, which is comparable with the 37.02% cloud cover for this flightline. These results confirm the MIR - snow cover relationship derived using the 9 February data.

DISCUSSION

Satellite-derived estimates of the snow and vegetation cover improve the understanding of the hydrologic, biogeochemical, and radiative interactions between the planetary surface and the atmosphere. This study shows that millimeter-wave radiation data can be used for detecting and monitoring snow and vegetation cover, particularly under cloudy conditions. This represents a distinct improvement over visible and near-infrared techniques which are unable to detect surface features under thick cloud. Furthermore, brightness temperature data near 89 GHz can be measured from space at a resolution of around 14 by 16 km, compared with around 45 by 70 km for 37 GHz. Hence, 89 GHz data have the potential for higher resolution snow-cover monitoring relative to the more commonly-used microwave frequencies.

Surface features such as coastlines, changes in vegetation between forests and cropland, and snow covered area are clearly discernible for cloud-free scenes in the millimeter-wave brightness temperature data, particularly at 89 GHz. In addition, there

is some indication that the MIR data can be used to estimate the percent forest cover. This is because as the percent forest cover increases, the proportion of emission from the trees increases resulting in higher brightness temperatures. During cloudy conditions, these surface features are still detectable. At 89 GHz, the difference between a cloudy and cloud-free snow-covered scene is only 2 K. This suggests that much of the microwave signal from the surface can penetrate the cloud cover without significant attenuation at this frequency.

A model for estimating the snow-covered area using 89 GHz MIR data was developed using brightness temperature cutoffs, adjusted for surface air temperature to account for variability in these data. It is shown that the MIR model compares well with the MODIS snow mapping algorithm under clear skies, and that it continues to perform when clouds are present, while the MODIS algorithm, which uses visible and near-infrared data, is unable to map snow under most clouds. The MIR method slightly underestimates snow cover under dense forest cover, due to the brightness temperature contribution from the canopy.

The air temperature data used in this study are at a resolution of 2.5 by 2.5 degrees. Future algorithm development should include data at a resolution more comparable with the microwave data. Surface temperature data, derived from MODIS data, may also be useful. These data, together with brightness temperature data, could be used to determine the surface emissivity, which is a more direct indicator of snow and vegetation cover.

CONCLUSIONS

Millimeter-wave radiation data is a useful addition to the multiple sources of information about the snow and vegetation cover of the planet. During the winter months, brightness temperature data at 89 GHz can be used to supplement visible and near-infrared methods of snow and vegetation detection which have a far better resolution but are hampered by the presence of cloud. Further studies are required to examine the utility of millimeter-wave data during other times of the year and for other locations. One such study, over Alaska in April 1995 (Tait *et al.*, submitted), concludes that 89 GHz data can be used to differentiate between gross changes in land cover, such as between vegetated and barren land, but that the data were significantly affected by the condition of the snowpack (dry, melting, or patchy). In addition, the Alaska study showed that some clouds were detectable using MIR data, and they effectively obscured the surface details.

It is concluded, therefore, that the use of millimeter-wave radiation data for detection of snow and vegetation cover varies with time of year and location. While it has been shown that the data are extremely useful for the Great Lakes, New England, and Ontario region in mid-winter, the results may be less applicable in the spring months in locations such as Alaska. A full analysis of the potential of millimeter-wave

for snow and vegetation cover detection using satellite-derived data covering several locations and several months is strongly suggested for future study.

ACKNOWLEDGMENTS

The authors wish to thank the following people and organizations for their help : Joan Ramage (Cornell University, Ithaca, NY), Alexandra Moore and Carrie Brindisi (Department of Geological and Environmental Sciences, Hartwick College, Oneonta, NY) and Klaus Bayr and students (Keene State College, Keene, NH) for gathering the field data; Paul Racette and Jim Wang (NASA / GSFC, Greenbelt, MD) for the collection and compilation of the MIR data; Crystal Schaaf (Boston University, Boston, MA) for the NOAA data and NOAA CDC (Boulder, CO) for the NCAR / NCEP Reanalysis data. This work is supported by the EOS / MODIS Snow and Ice Project.

REFERENCES

Ackerman, S.; Strabala, K.; Menzel, P.; Frey, R.; Moeller, C.; Gumley, L.; Baum, B.; Schaaf, C. and Riggs, G. (1997) *Discriminating clear-sky from cloud with MODIS.* Algorithm theoretical basis document, Version 3.2 (MOD35), 131pp.

Allen, R.C. (Jr.); Durkee, P.A. and Wash, C.H. (1990) Snow / cloud discrimination with multispectral satellite measurements. *Journal of Applied Meteorology*, 29, p 994-1004.

Belward, A.S. and Loveland, T.R. (1995) The IGBP-DIS 1km Land Cover Project : Remote sensing in action. In *Proceedings of the 21st annual conference of the Remote Sensing Society*, Southampton, UK, p 1099-1106.

Chang, A.T.C.; Foster, J.L.; Owe, M.; Hall, D.K. and Rango, A. (1985) Passive and active microwave studies of wet snowpack properties. *Nordic Hydrology*, 16, p 57-66.

Chang, A.T.C.; Foster, J.L. and Hall, D.K. (1987) Microwave snow signatures (1.5mm to 3cm) over Alaska. *Cold Regions Science and Technology*, 13, p 153-160.

Gasiewski, A.J. (1992) Numerical sensitivity analysis of passive EHF and SMMW

channels to tropospheric clouds, water vapor, and precipitation. *IEEE Transactions of Geoscience and Remote Sensing*, 30, p 859-870.

Hahn, D.G. and Shukla, J. (1976) An apparent relationship between Eurasian snow cover and Indian monsoon rainfall. *Journal of Applied Sciences*, 33(12), p 2461-2462.

Hall, D.K.; Foster, J.L.; Chang, A.T.C.; Benson, C.S. and Chien, J.Y.L. (1995) Determination of snow-covered area in different land covers in central Alaska, U.S.A., from aircraft data - April 1995. *Annals of Glaciology*, 26, in press.

IGBP (International Geosphere-Biosphere Programme) (1990) The Initial Core Projects. IGBP Report No. 12, Stockholm, Sweden.

Klein, A.G.; Hall, D.K. and Riggs, G.A. (1998) Improving snow-cover mapping in forests through the use of a canopy reflectance model. *Hydrological Processes*, in press.

Massom, R. (1991) *Satellite Remote Sensing of Polar Regions*. Belhaven Press, London, 307pp.

Racette, P.; Adler, R.F.; Wang, J.R.; Gasiewski, A.J.; Jackson, D.M. and Zacharias,

D.S. (1996) An airborne millimeter-wave imaging radiometer for cloud, precipitation, and atmospheric water vapor studies. *Journal of Atmospheric and Oceanic Technology*, 13(3), p 610-619.

Rango, A.; Chang, A.T.C. and Foster, J.L. (1979) The utilization of space-borne microwave radiometers for monitoring snowpack properties. *Nordic Hydrology*, 10, p 25-40.

Rango, A. (1985) An international perspective on large-scale snow studies. *Hydrological Sciences Journal*, 30, p 225-238.

Reeves, R.G.; Anson, A. and Landen, D. (eds) (1975) *Manual of Remote Sensing.* American Society of Photogrammetry, Falls Church, VA, 867pp.

Tait, A.B.; Hall, D.K.; Foster, J.L. and Chang, A.T.C. (submitted) High frequency passive microwave radiometry over a snow-covered surface in Alaska. Submitted to *Photogrammetric Engineering and Remote Sensing.*

Townshend, J.R.G.; Tucker, C.J. and Goward, S.N. (1993) Global vegetation mapping. In Gurney, R.J.; Foster, J.L. and Parkinson, C.L. (eds) *Atlas of Satellite Observations Related to Global Change.* Cambridge University Press, New York, p 301-311.

Ulaby, F.T. and Stiles, W.H. (1980) Microwave radiometric observations of snowpacks, NASA CP-2153. In *NASA Workshop on the Microwave Remote Sensing of Snowpack Properties*, Ft. Collins, CO, 20-22 May, p 187-201.

Walsh, J.E. and Ross, B. (1988) Sensitivity of 30-day forecasts to continental snow cover. *Journal of Climatology*, 1, p 739-754.

LIST OF FIGURES

Figure 7 : The difference between the number of snow-covered pixels per scan line computed from the MIR and MAS algorithms for 9 February 1997.

Figure 8 : The difference between the number of snow-covered pixels per scan line computed from the MIR and MAS algorithms for 6 February 1997.

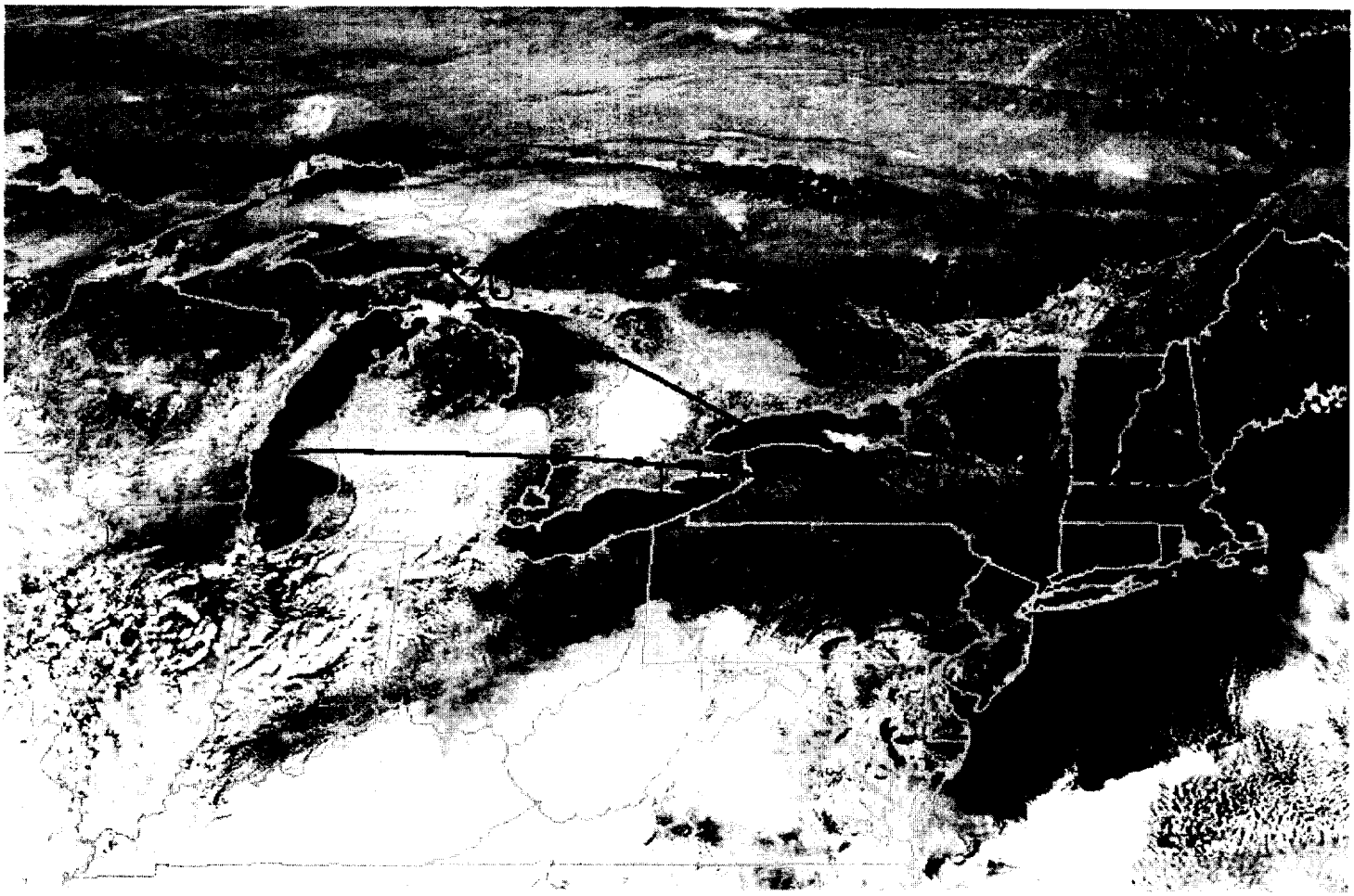

Figure 1

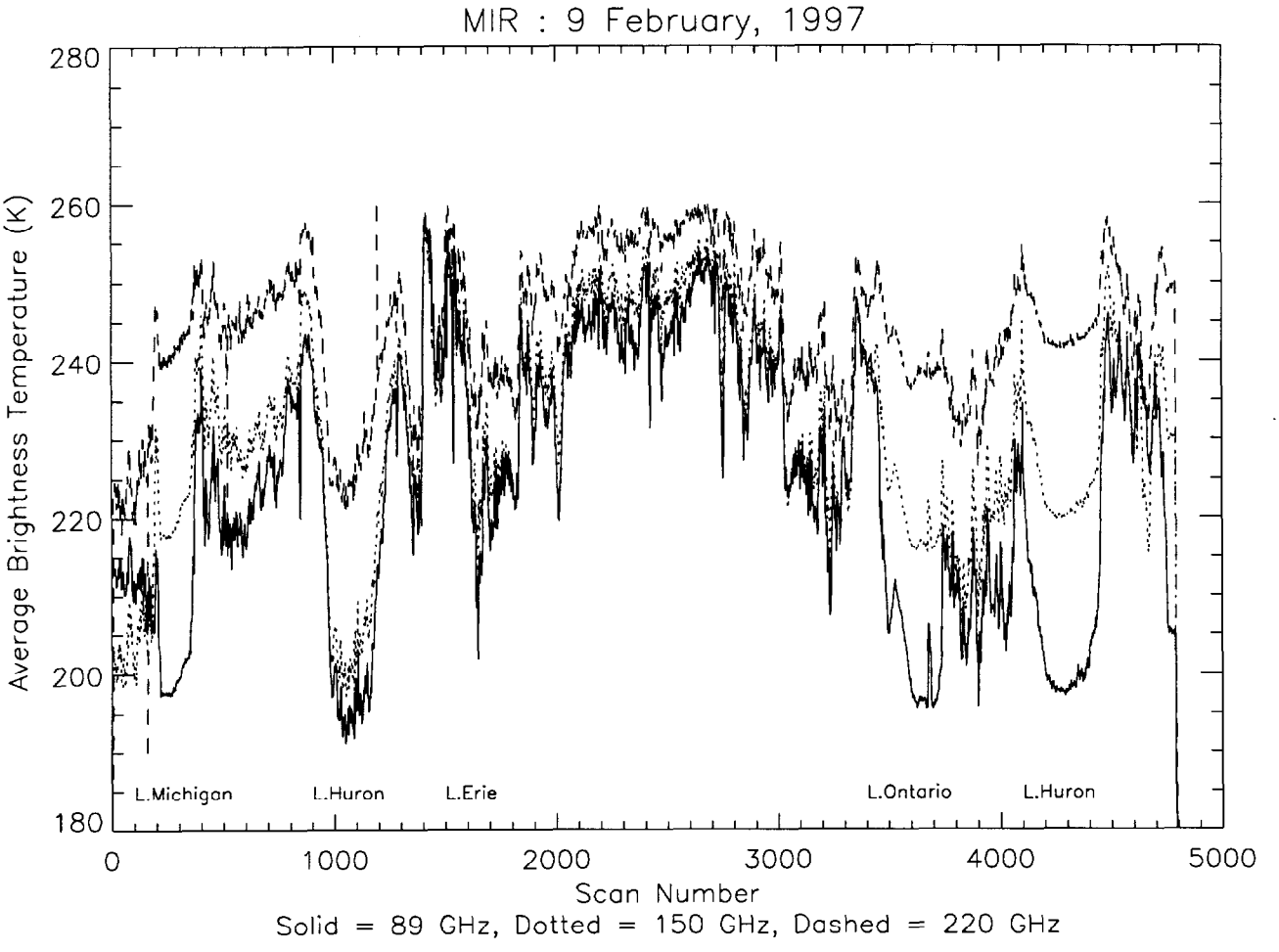
MIR : 9 February, 1997
Average Brightness Temperature (K)
280
260
240
220
200
180
0
1000
2000
3000
4000
5000
Scan Number
L.Michigan
L.Huron
L.Erie
L.Ontario
L.Huron
Solid = 89 GHz, Dotted = 150 GHz, Dashed = 220 GHz

Figure 2

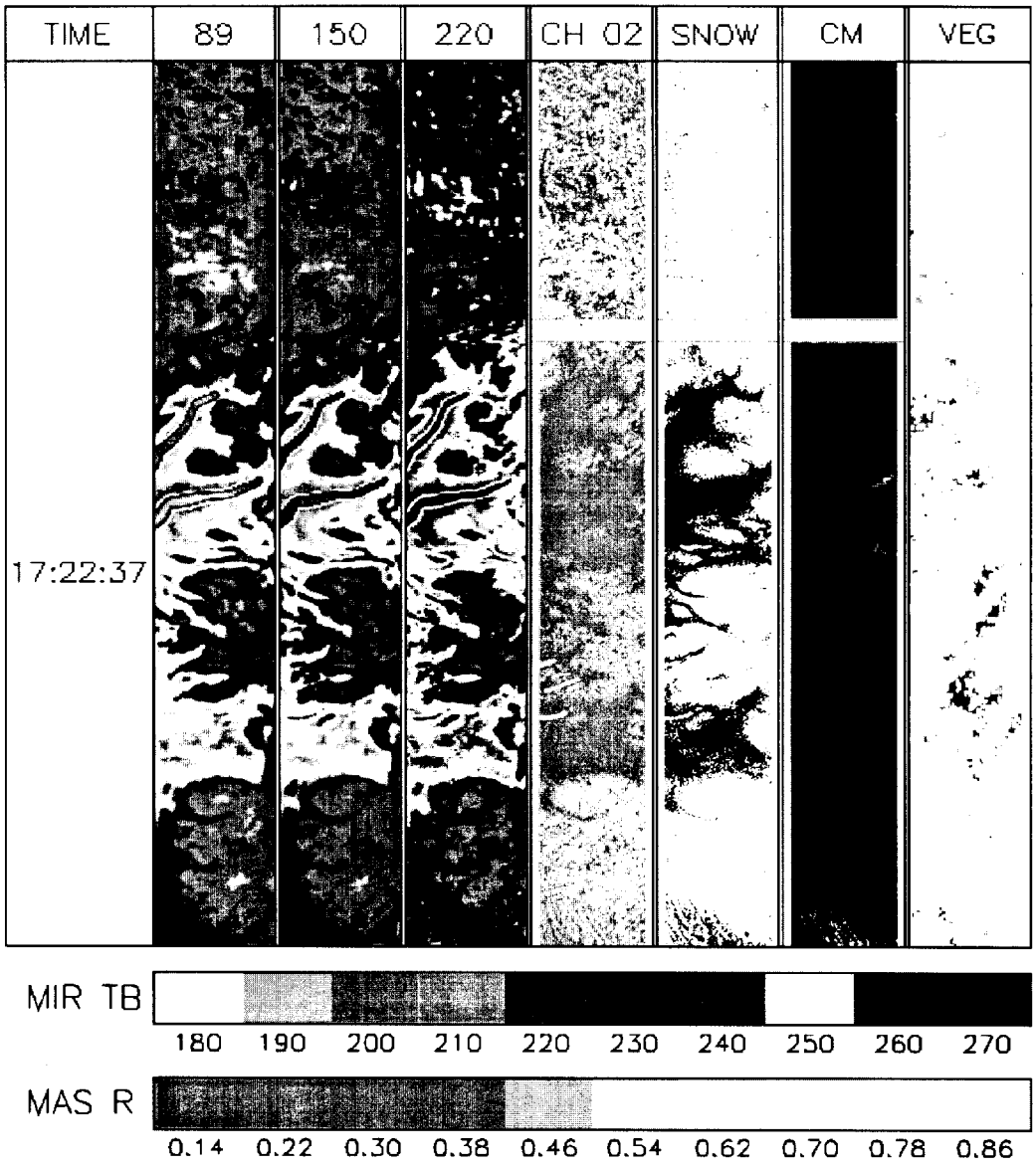
TIME
89
150
220
CH 02
SNOW
CM
VEG
17:22:37
MIR TB
180 190 200 210 220 230 240 250 260 270
MAS R
0.14 0.22 0.30 0.38 0.46 0.54 0.62 0.70 0.78 0.86

Figure 3

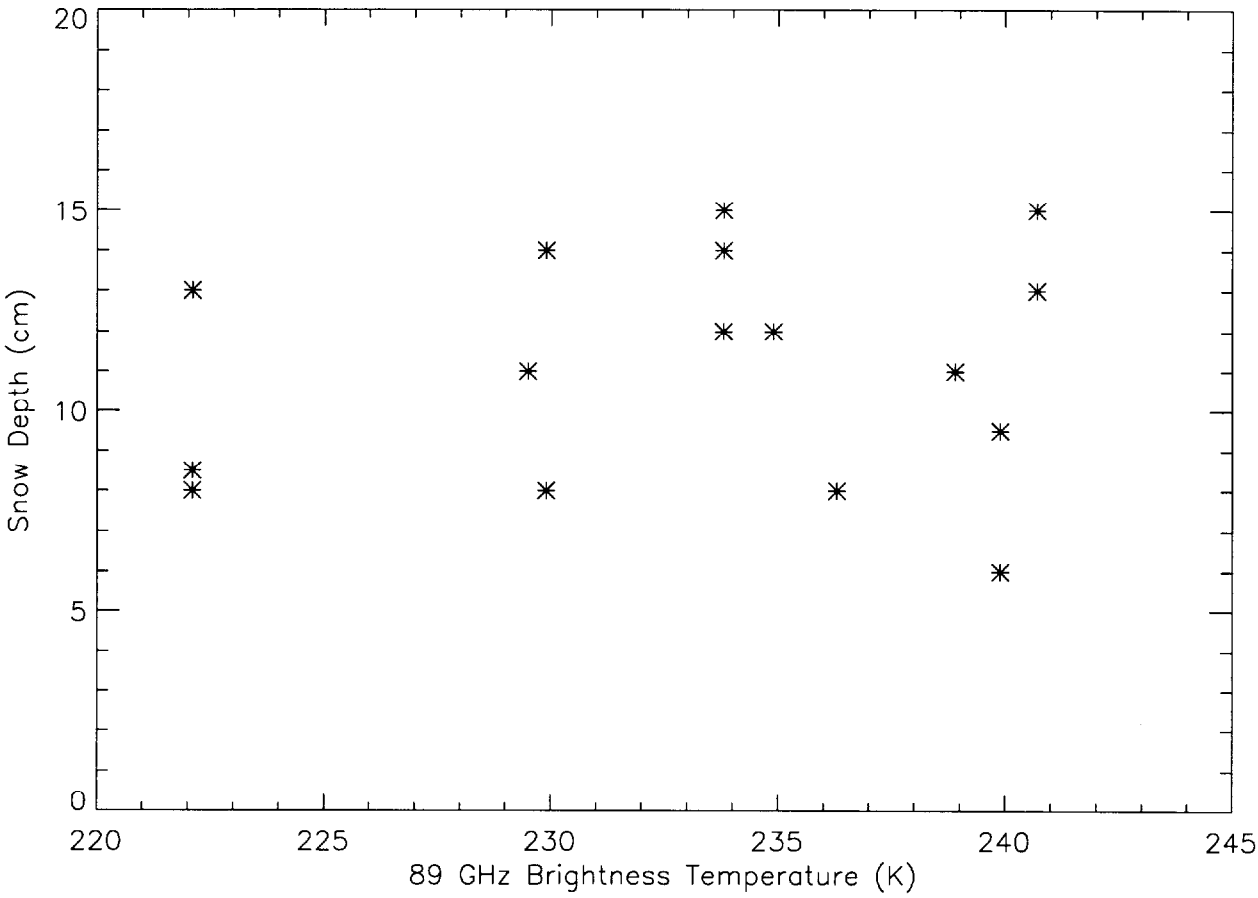
20
15
10
5
0
Snow Depth (cm)
220
225
230
235
240
245
89 GHz Brightness Temperature (K)

Figure 4

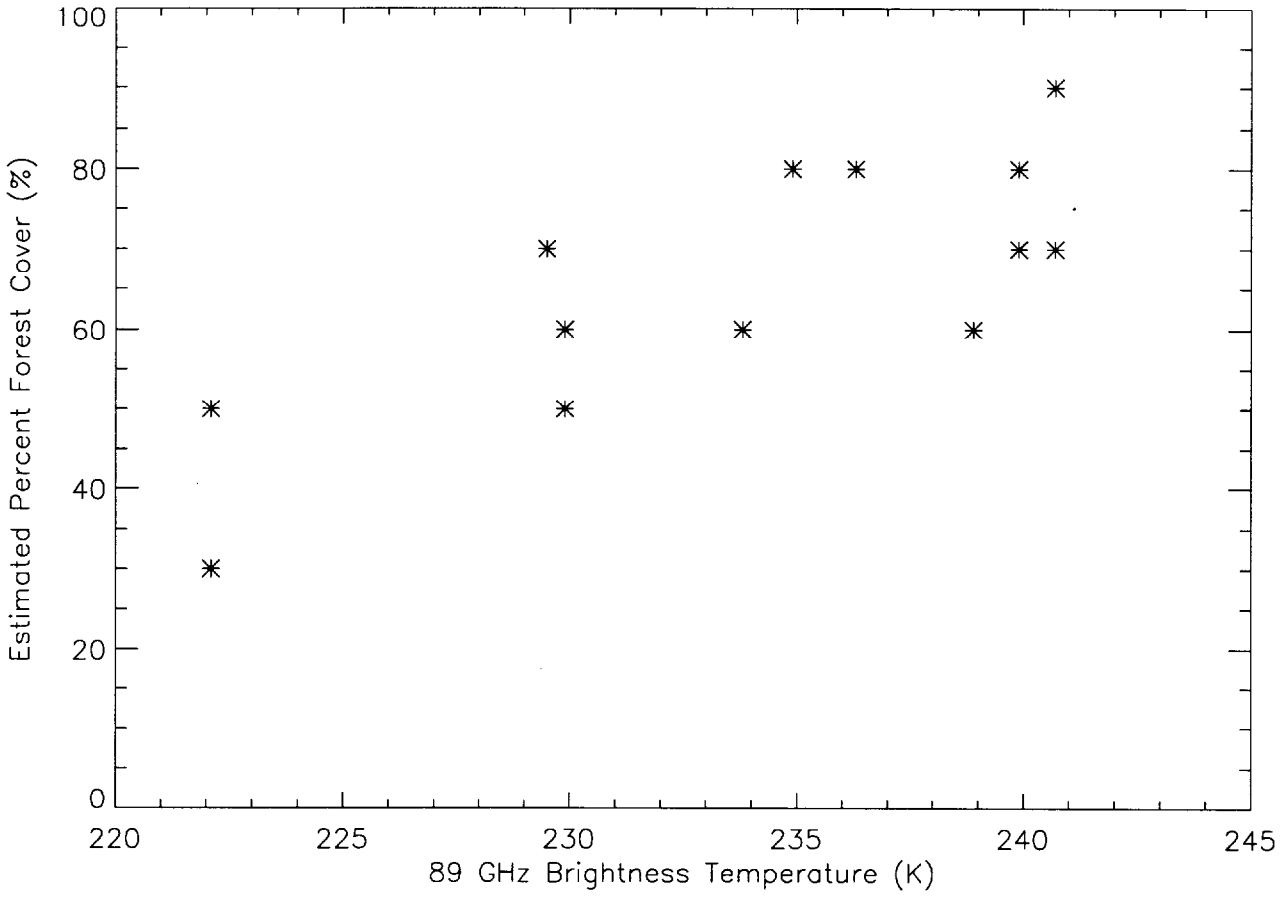
100
80
60
40
20
0
Estimated Percent Forest Cover (%)
220
225
230
235
240
245
89 GHz Brightness Temperature (K)

Figure 5

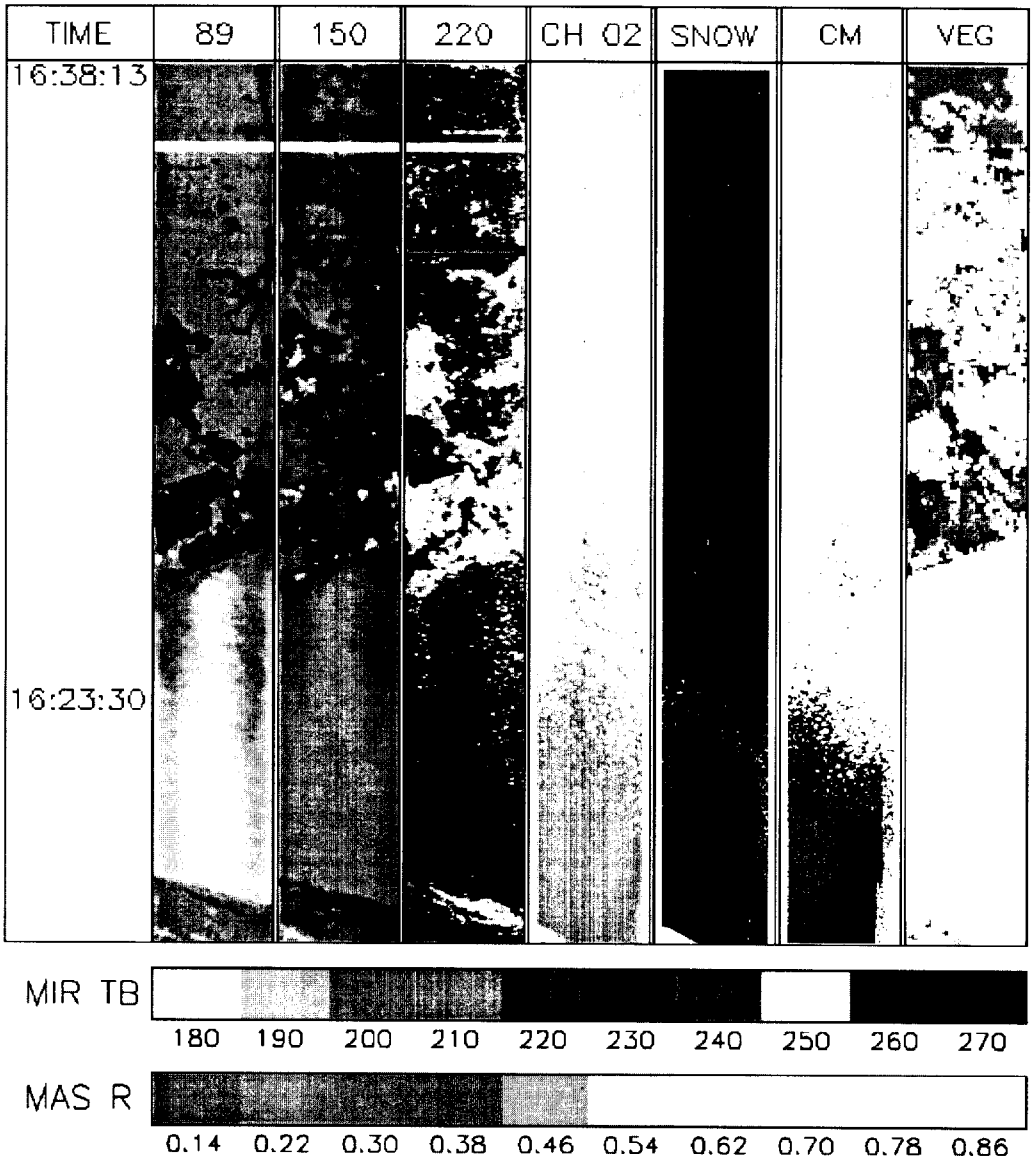
TIME
89
150
220
CH 02
SNOW
CM
VEG
16:38:13
16:23:30
MIR TB
180 190 200 210 220 230 240 250 260 270
MAS R
0.14 0.22 0.30 0.38 0.46 0.54 0.62 0.70 0.78 0.86

Figure 6

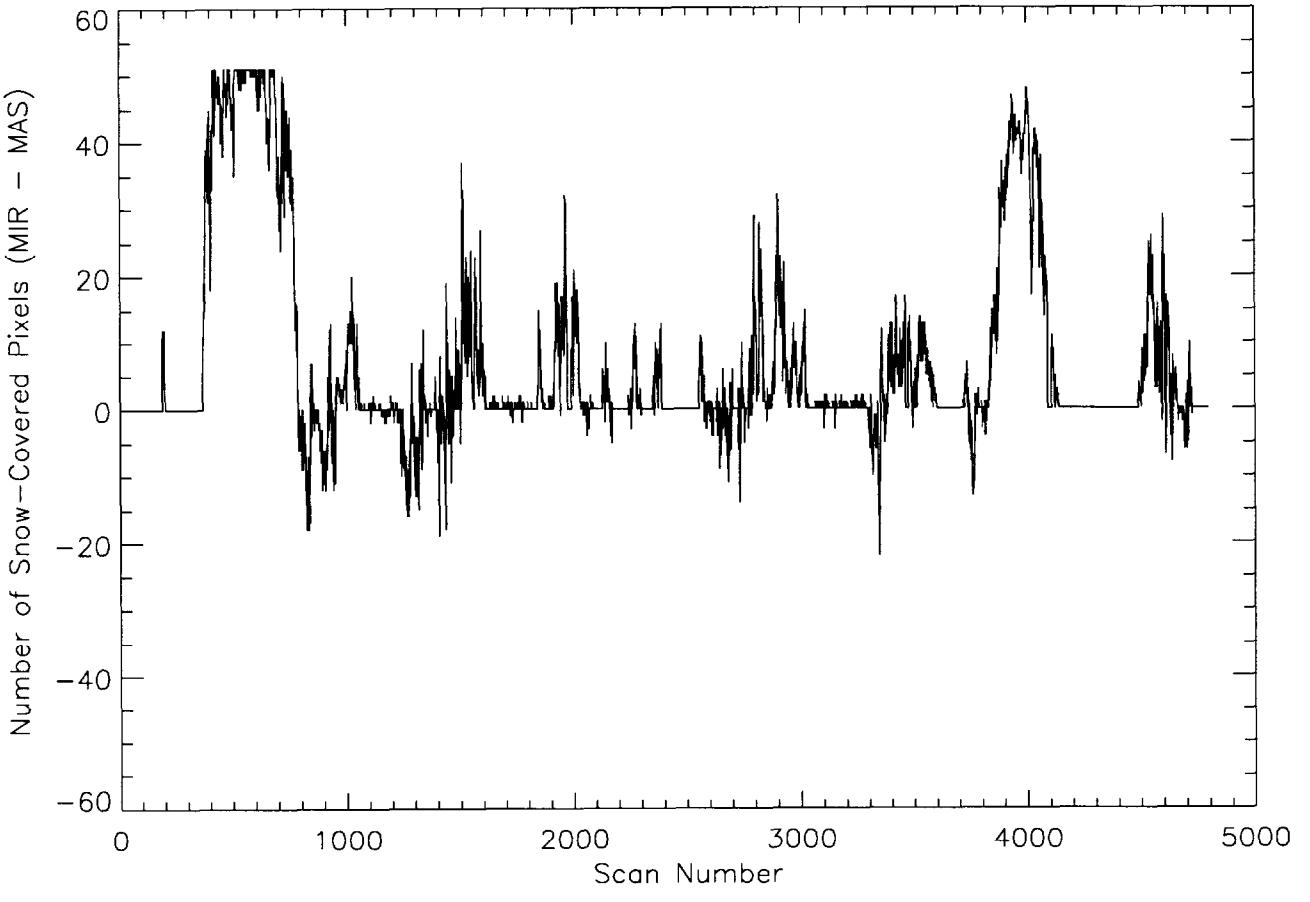
60
40
20
0
−20
−40
−60
0
1000
2000
3000
4000
5000
Scan Number
Number of Snow−Covered Pixels (MIR − MAS)

Figure 7

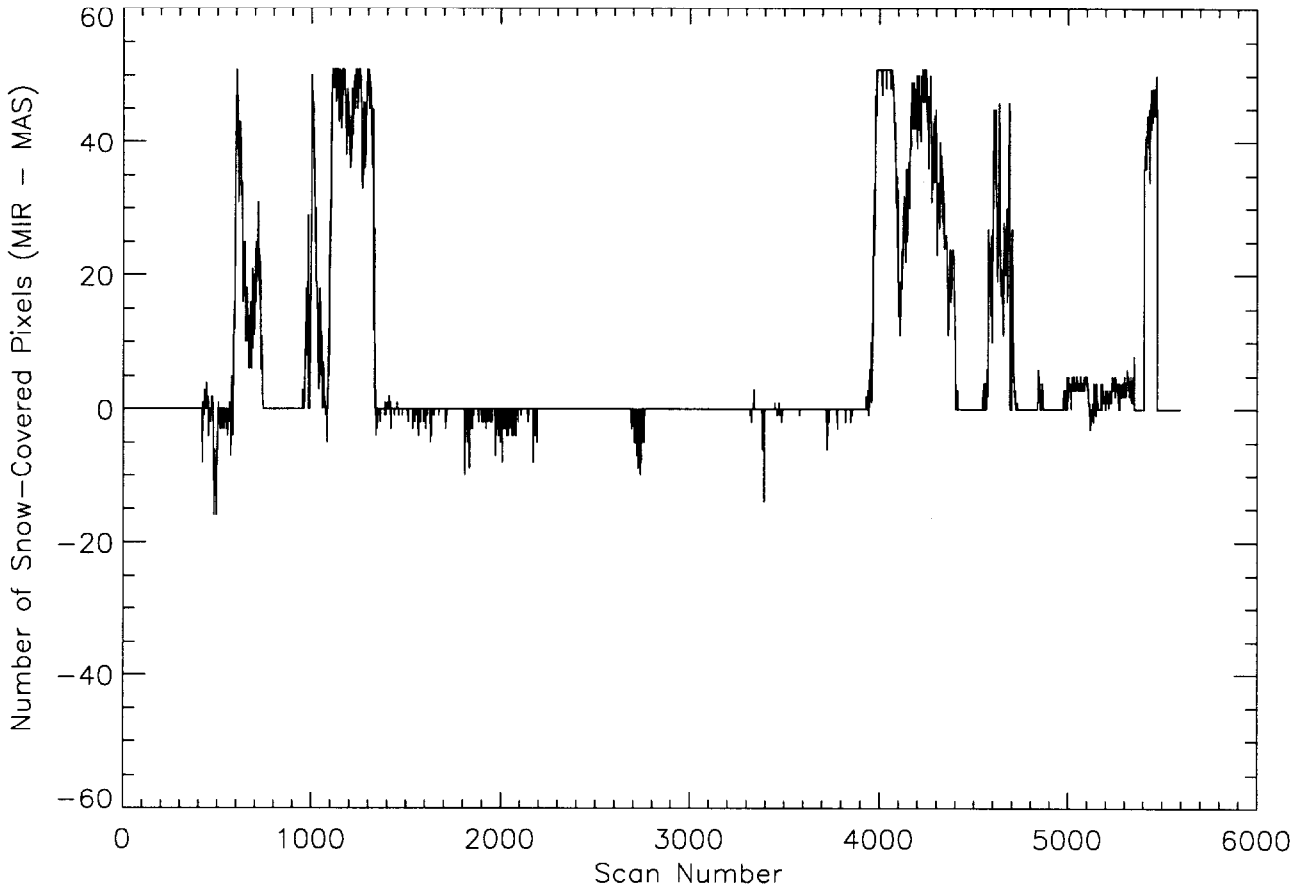
60
40
20
0
−20
−40
−60
0
1000
2000
3000
4000
5000
6000
Number of Snow−Covered Pixels (MIR − MAS)
Scan Number

Figure 8

Table 1 : Characteristics of the MIR receiver channels (from Racette *et al.*, 1996).

Channel	Wavelength Range (mm)	Frequency Range (GHz)	Sensitivity (K)
1	3.371 +- 0.038	89.0 +- 1.0	0.13
2	2.000 +- 0.013	150.0 +- 1.0	0.13
3	1.637 +- 0.009	183.3 +- 1.0	0.39
4	1.637 +- 0.027	183.3 +- 3.0	0.39
5	1.637 +- 0.065	183.3 +- 7.0	0.31
6	1.364 +- 0.006	220.0 +- 2.5	0.32
7	0.923 +- 0.003	325.0 +- 1.0	~ 8
8	0.923 +- 0.009	325.0 +- 3.0	~ 8
9	0.923 +- 0.022	325.0 +- 8.0	~ 8

Table 2 : Oneonta NY field data and MIR 89 GHz brightness temperatures

Site	Latitude	Longitude	Snow Depth (cm)	Tree Density (%)	TB 89 GHz (K)
1	42.450	74.931	8	60	229.9
2	42.451	74.932	8	50	222.1
3	42.451	74.933	8.5	50	222.1
4	42.453	74.933	13	30	222.1
5	42.455	74.932	14	50	229.9
6	42.456	74.931	11	70	229.5
7	42.458	74.930	9.5	70	239.9
8	42.459	74.929	6	80	239.9
9	42.461	74.928	9.5	70	239.9
10	42.462	74.927	12	80	234.9
11	42.464	74.928	8	80	236.3
12	42.465	74.927	15	60	233.8
13	42.467	74.928	11	60	238.9
14	42.468	74.926	12	60	233.8
15	42.469	74.926	14	60	233.8
16	42.472	74.925	15	70	240.7
17	42.475	74.926	13	90	240.7